Chemical Science

ROYAL SOCIETY OF CHEMISTRY

EDGE ARTICLE

Check for updates

All publication charges for this article have been paid for by the Royal Society of Chemistry

Light-harvesting complexes access analogue emissive states in different environments†

Vincenzo Mascoli,[a] Andrius Gelzinis,[bc] Jevgenij Chmeliov, [ID] [bc] Leonas Valkunas[bc] and Roberta Croce [ID] *[a]

The light-harvesting complexes (LHCs) of plants can regulate the level of excitation in the photosynthetic membrane under fluctuating light by switching between different functional states with distinct fluorescence properties. One of the most fascinating yet obscure aspects of this regulation is how the vast conformational landscape of LHCs is modulated in different environments. Indeed, while in isolated antennae the highly fluorescent light-harvesting conformation dominates, LHC aggregates display strong fluorescence quenching, representing therefore a model system for the process of energy dissipation developed by plants to avoid photodamage in high light. This marked difference between the isolated and oligomeric conditions has led to the widespread belief that aggregation is the trigger for the photoprotective state of LHCs. Here, a detailed analysis of time-resolved fluorescence experiments performed on aggregates of CP29 – a minor LHC of plants – provides new insights into the heterogeneity of emissive states of this antenna. A comparison with the data on isolated CP29 reveals that, though aggregation can stabilize short-lived conformations to a certain extent, the massive quenching upon protein clustering is mainly achieved by energetic connectivity between complexes that maintain the same long-lived and dissipative states accessed in the isolated form. Our results also explain the typical far-red enhancement in the emission of antenna oligomers in terms of a sub-population of long-lived redshifted complexes competing with quenched complexes in the energy trapping. Finally, the role of selected chlorophylls in shaping the conformational landscape of the antenna is also addressed by studying mutants lacking specific pigments.

Introduction

In the photosynthetic organisms of green lineage, light-harvesting complexes (LHCs) are membrane-embedded proteins that bind pigment molecules—chlorophylls (Chls) and carotenoids (Cars)—and whose ultimate role is to increase the absorption cross-section for charge separation, the primary step of photosynthetic reactions. The LHCs of plants and algae belong to the same gene superfamily[1] and are highly homologous. However, they possess a high degree of tunability of pigment–protein and pigment–pigment interactions, which reflects into their vast conformational landscape and, consequently, into a wide range of excited state properties for their chlorophylls. These antennae are therefore able to switch between different emissive states, marked by distinct fluorescence spectra and chlorophyll excited state lifetimes,[2–6] a property that is essential to regulate and balance the amount of excitation in the photosynthetic membranes in response to changes in light intensity.[7–9] While a long-lived state is required in low light to maximize the efficiency of energy transport towards the reaction center (RC), a short-lived (quenched) state is needed to safely dissipate the excess energy absorbed in high light to avoid photodamage. Furthermore, the emission wavelengths of chlorophylls can be shifted across a broad spectral range in the visible red and near infrared.[10–13] The LHCs of photosystem (PS) II (also called LHCb's) of plants and algae, for instance, are substantially found in a fluorescent state emitting around 680 nm,[14,15] whereas the antennae of PSI (LHCa's) largely emit at longer wavelengths, from 690 up to 740 nm.[16]

The above-mentioned heterogeneity of LHCs has been probed in multiple works using single-molecule[4,17–19] and bulk[5,6,20–23] spectroscopic techniques. However, the fine molecular details responsible for the switch between different states are not well understood. Furthermore, it is not clear how this diverse landscape responds to distinct external conditions. Do the LHCs adopt the same quenching mechanism in different environments? And how is the extent of their quenching

[a]Department of Physics and Astronomy and Institute for Lasers, Life and Biophotonics, Faculty of Sciences, Vrije Universiteit Amsterdam, De Boelelaan 1081, 1081 HV Amsterdam, The Netherlands. E-mail: r.croce@vu.nl

[b]Institute of Chemical Physics, Faculty of Physics, Vilnius University, Sauletekio Ave. 9, LT-10222 Vilnius, Lithuania

[c]Department of Molecular Compound Physics, Center for Physical Sciences and Technology, Sauletekio Ave. 3, LT-10257 Vilnius, Lithuania

modulated? The most relevant system to conduct this investigation is the thylakoid membrane. This represents, however, an extremely challenging sample, as the presence of reaction centers and of two types of photosystems results in very complex excited state dynamics, where it is virtually impossible to isolate contributions from a single LHC unit. On the other hand, several studies have demonstrated that the excited state dynamics of LHC aggregates *in vitro* share many spectroscopic signatures with *in vivo* quenching.[23–26] Indeed, while isolated LHCs are found mainly in a long-lived state functional for light harvesting,[20,21] aggregation is well known to decrease their fluorescence quantum yield[27] by shortening the chlorophyll excited state lifetime.[6,20,21,28,29] A detailed spectroscopic investigation of LHC aggregates, however, is hindered by the high number of energetically connected pigments, which poses additional experimental challenges.[30,31] In addition, the excited state kinetics of these large and heterogeneous systems become non-exponential due to diffusive processes[32] and incorporate signatures from multiple spectral forms, which further complicates their interpretation.[6,26,33] One of the long-standing controversies about quenching in the aggregates concerns the origin of the increased far-red emission observed upon clustering.[26,27,34] This observation has been sometimes used to suggest that redshifted states are involved in the aggregate quenching.[26,30,35] This interpretation, however, is at variance with experimental evidence from the LHCa's, whose red-emitting states are mostly long-lived.[36] At the same time, two recent works on aggregates of LHCII (the major LHC of plants and algae) pointed out that red-emitting states cannot be responsible for quenching, which was instead ascribed to an undetermined dark (non-fluorescent) state.[6,33] A number of studies[22,25,37,38] have proposed excitation energy transfer from chlorophylls to a short-lived carotenoid dark state as a viable candidate for the latter mechanism.

To date, time-resolved spectroscopic investigations of aggregation quenching have been substantially restricted to oligomers of LHCII *in vitro*[6,25] or to LHC clusters in the thylakoid membrane,[23,39] where LHCII is by far the most abundant antenna. However, the fact that the light-harvesting conformation is overwhelming in detergent-solubilized LHCII trimers[6,20] has hindered the comparison between the isolated and oligomeric conditions. In order to trace a connection between these two environments, this study addresses a different LHC, the minor antenna of plants CP29. As for LHCII trimers, monomeric CP29 (whose structure, shown in Fig. 1, is very similar to that of monomeric LHCII[40,41]) preferentially adopts a light-harvesting conformation. However, a significant minority of detergent-solubilized complexes (about 15%) can be found in a markedly dissipative state. This property of monomeric CP29 facilitates the investigation of its quenching mechanism, which was recently assigned to energy transfer from chlorophylls to a dark state of lutein *via* transient absorption (TA) measurements.[22] To assess whether the same quenching mechanism is also functional upon protein clustering and (if true) to which extent it is regulated, the excited state dynamics of CP29 aggregates is here probed *via* time-resolved fluorescence (TRF). This technique allows measurements of the oligomers at the
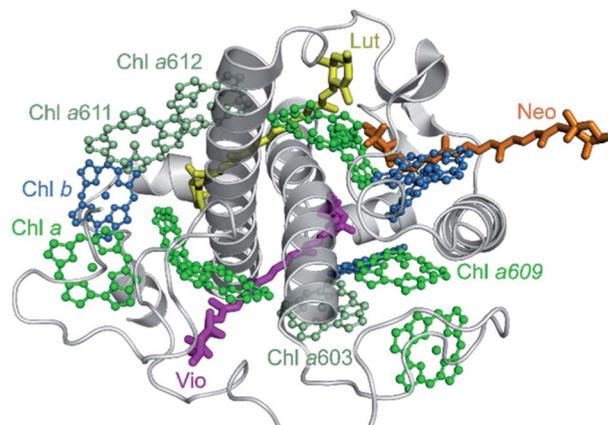

Fig. 1 Crystal structure of CP29 complex from the PDB file 5XNL[41] exhibiting 10 Chls *a* (green), 4 Chls *b* (blue), and 3 carotenoids—lutein (yellow), violaxanthin (magenta) and neoxanthin (orange)—bound to the protein scaffold (grey). For clarity, only chlorin rings of the Chl pigments are shown. Chls *a*603 as well as *a*611 and *a*612, that are absent in the KO603 and KO612 mutants, respectively (see text below), are indicated explicitly with slightly different color.

relatively low laser powers that are imperative to avoid power-dependent artefacts,[6,31] while those would be nearly unavoidable at the higher powers needed for TA. TRF measurements permit to relate the quenching in the monomers to that in the oligomers based on their fluorescence signatures (spectrum, lifetime, occurrence and trapping strength) while avoiding kinetics artifacts.

The work is organized as follows: we first present TRF data (and the results from their global analysis) of native CP29 at room and cryogenic temperatures and comment about general spectral/temporal trends. We successively perform a decomposition of the same data to extract the spectroscopic signatures of the different emissive states present in the aggregates. The results from this decomposition are then used as input for a model-based fit to obtain more insights on the thermodynamic and kinetic properties of these fluorescent states and, more specifically, on the mechanism responsible for quenching. Finally, the same methodology is applied to two chlorophyll-deficient mutants of CP29 (ref. 42) to shed light on the role of specific chlorophylls in the occurrence and regulation of the observed states.

Methods

Sample preparation

Monomeric CP29 and its chlorophyll knock-out mutants were isolated from *Arabidopsis thaliana* as described in Xu *et al.*[42] For measurements on monomeric CP29, the sample was diluted to the desired OD in a buffer of HEPES 10 mM (pH ~ 7.5) and 0.03% alpha-DM. For measurements in the oligomeric state, samples were diluted to the desired OD in a buffer of HEPES 10 mM (pH ~ 7.5) and 0.003% alpha-DM (*i.e.* below the critical micellar concentration of alpha-DM of about 0.008–0.01%). All samples were incubated for 4 hours after detergent dilution from 0.03% to 0.003% (at 4 °C and gently shaking to avoid

precipitation) and one more hour at RT in the measuring cuvette (magnetically stirred with a speed of 1200 rpm). This protocol allowed for 1 hour long fluorescence measurements on a sample with a stable level of aggregation (see Fig. S1†). Measurements were performed on 3 biological replicas, yielding a relative standard error ≤ 10% on the average fluorescence lifetime of the aggregates at RT.

Experiments were also performed at other detergent concentrations (data not shown) and resulted in qualitatively similar fluorescence kinetics, the only relevant difference being the amount of residual unconnected antenna. Our results on CP29 clusters obtained by detergent dilution also agree qualitatively with those from a previous study on LHCII, where oligomers were obtained *via* bio-absorbent beads. These pieces of evidence indicate that the photophysics of antenna oligomers are fundamentally independent on the preparation method.

Steady-state and time-resolved fluorescence

Room-temperature fluorescence emission spectra were acquired at an OD < 0.05 cm^{-1} on a HORIBA Jobin-Yvon FluoroLog-3 spectrofluorometer. 77 K emission spectra were measured using a liquid nitrogen cooled device (cold finger).

TRF on CP29 monomers at 77 K was measured *via* time-correlated single photon counting (TCSPC) on a FluoTime 200 from PicoQuant using a liquid nitrogen cooled device (cold finger). The excitation wavelength was 468 nm for all measurements, with a power of 100 µW and a repetition rate of 10 MHz. The OD of all samples was <0.05 cm^{-1}. Under these conditions, no power dependency was observed. The signal was acquired at different wavelengths for 10 minutes (or until a number of 10 000 counts at peak maximum was reached), using a time window of 20 ns and a time bin of 4 ps.

TRF on CP29 aggregates was recorded with a Hamamatsu C5680 synchro scan streak camera, combined with a Chromex 250IS spectrograph. A grating of 50 grooves per mm and a blazed wavelength of 600 nm was used for all measurements and the central wavelength was set to 680 nm, with each image covering a spectral width of 260 nm. The excitation wavelength was 400 nm and the laser repetition rate was 250 kHz. The excitation beam was vertically polarized, with the spot size diameter in the order of 100 µm. A time window of 1.5 ns was used and each measurement contains 60 minutes of CCD exposure time in total. Approximately 0.5 mL samples with OD < 0.6 cm^{-1} were measured at RT in a magnetically stirred 1 cm × 1 cm cuvette (speed of 1200 rpm). 77 K experiments were performed using a liquid nitrogen cooled device (cold finger). The power dependency of the measured fluorescence kinetics was tested in order to perform all measurements in annihilation-free conditions (see power study in Fig. S2†). All data were obtained with an excitation power ≤50 µW at RT and ≤25 µW at 77 K. Additional care was taken to avoid significant reabsorption in the measurements. The averaged images were corrected for background and shading, and then sliced into traces of ∼1 nm width (∼2 nm for the KO603 samples to compensate for the lower signal-to-noise ratio resulting from the lower sample concentration).

Data analysis

Fluorescence time traces were globally analyzed using a number of parallel, non-interacting kinetic components, so that the total dataset can be described by the convolution of the instrument response function (IRF) with the sum of exponentially decaying spectral components

$$F(t,\lambda) = \sum_{k=1}^{n} \text{DAS}_k(\lambda) \, \exp\left(-\frac{t}{\tau_k}\right) \otimes \text{IRF}(t,\lambda)$$

where each decay-associated spectrum (DAS$_k$) is the amplitude factor associated with a decay component k having a decay lifetime τ_k. The instrument response function IRF(t,λ) was estimated from the fitting in the case of streak camera measurements (FWHM ∼ 20 ps) and *via* the measured decay of pinacyanol iodide in methanol at RT (lifetime of around 6 ps)[43] for TCSPC measurements (FWHM ∼ 90 ps). The EAS were obtained similarly, with populations being obtained from a sequential kinetic model. Note that, for all streak camera data, the global analysis also corrects for the time-zero dispersion.

For TCSPC data, the fitting quality was assessed by the χ^2 value and by residual inspection. More details about the global analysis methods can be found in van Stokkum *et al.*[44]

The excited state kinetics in the aggregates of CP29 at both temperatures were analyzed in terms of multivariate curve resolution as previously reported for LHCII aggregates.[6] This approach allows to extract a minimal number of fluorescent states from the data matrix $F(t,\lambda)$, each provided with a spectrum (species associated spectrum, SAS(λ)) and a kinetic trace $C(t)$ according to the equation:

$$F(t,\lambda) = \sum_{k}^{N} \text{SAS}_k(\lambda) C_k(t)$$

where N is the number of components required for an adequate fitting. With this strategy, we could distinguish between the population kinetics of the different spectral components in the aggregate (blue, intermediate and far-red, see Fig. 4, S20, S21, S25 and S26†). The minimal number of components N needed for the fitting was estimated from Singular Value Decomposition (as the number of independent components above the noise level, see caption of Fig. S5† for more details).

The extracted kinetics were then used as a reference in our coarse-grained simulations in order to extract other relevant parameters, such as the relative amounts of the different emissive states in the aggregate, the rates of energy transfer between them and the lifetime of the dissipative state. We used the same fitting procedure as in Chmeliov *et al.*,[6] but few changes were implemented to account for the specificity of the samples used here (see ESI Text S1† for details).

Results

Time-resolved fluorescence measurements on CP29 aggregates

Here we present TRF data of CP29 oligomers and compare them to the data of CP29 monomers, which can be found in the ESI.† Protein clustering induces a drastic shortening of the

chlorophyll excited state lifetime. At room temperature (RT), the fluorescence trace detected at 680 nm of CP29 aggregates decays with an average lifetime of less than 200 ps (the monomers have an average lifetime of 3.1 ns at RT, see Fig. S3d†). Global analysis of the RT TRF data (which are shown in Fig. 2a) reveals that, after some fast downhill energy transfer (Fig. 2b, black DAS), two main decay components are present: a faster one (74 ps, red DAS in Fig. 2b), and a slower one (200 ps, blue DAS). The very small long-lived component peaking at 674 nm (green DAS in Fig. 2b) is due to a minor fraction of unconnected pigments/antennae. Notably, although the two major decay components both peak around 680 nm, they have a different spectrum, the slower component being broader and more pronounced in the far-red region. Consequently, the average lifetime has a minimum at 680 nm and increases at longer wavelengths, with a maximum near 720 nm (Fig. 2c). This results in a time-integrated (steady-state) fluorescence spectrum of the aggregates with an enhanced far-red contribution (Fig. 2d) in comparison to monomeric CP29 (whose average lifetime is, instead, rather insensitive to the emission wavelength, compare Fig. 2c and S3d†). These findings prove that energy trapping in oligomeric CP29 exhibits fast heterogeneous kinetics and is slowed down at longer wavelengths (see also Fig. S4g†).

The wavelength-dependency of the aggregate lifetime and the kinetic heterogeneity become more evident at lower temperature (Fig. 3a). At 77 K, the fluorescence emitted at 700 nm is sizably longer-lived than that at 680 nm (Fig. 3b).

Furthermore, the fluorescence spectrum at 1 ns time delay is clearly redshifted in comparison to the spectrum immediately after excitation (Fig. 3c), as previously observed for LHCII oligomers at low temperatures.[6] Global analysis reveals that the excited state kinetics of aggregated CP29 involve several steps on multiple timescales (Fig. 3d, S4d and f†): the first two DAS in Fig. 3d have non-conservative amplitude, which indicates that both downhill energy equilibration and excited state relaxation are taking place in 17 and 74 ps, resulting in the decay of the largest part of the fluorescence signal. The two slower DAS show that the residual fluorescence is emitted from redshifted states in hundreds of picoseconds or even nanoseconds. The resulting average lifetime increases from about 0.1 ns at 680 nm to almost 1.5 ns at 710 nm (Fig. 3e). Due to the strong wavelength dependence of the average lifetime, the integrated fluorescence of aggregated CP29 at 77 K has a peak at 705 nm, with a shoulder at shorter wavelengths due to short-lived fluorescence at 680 nm immediately after excitation (Fig. 3f).

Experimental data support a heterogeneous picture

The excited state kinetics in the aggregates contain contributions from a large amount of energetically connected pigments/antennae and display a marked spectral heterogeneity. As a result of the aggregate size, energy transfer is expected to follow a diffusive regime where a kinetic analysis in terms of DAS and exponential decays was shown not to be appropriate.[6,45,46] The current CP29 data reveal fluorescence kinetics
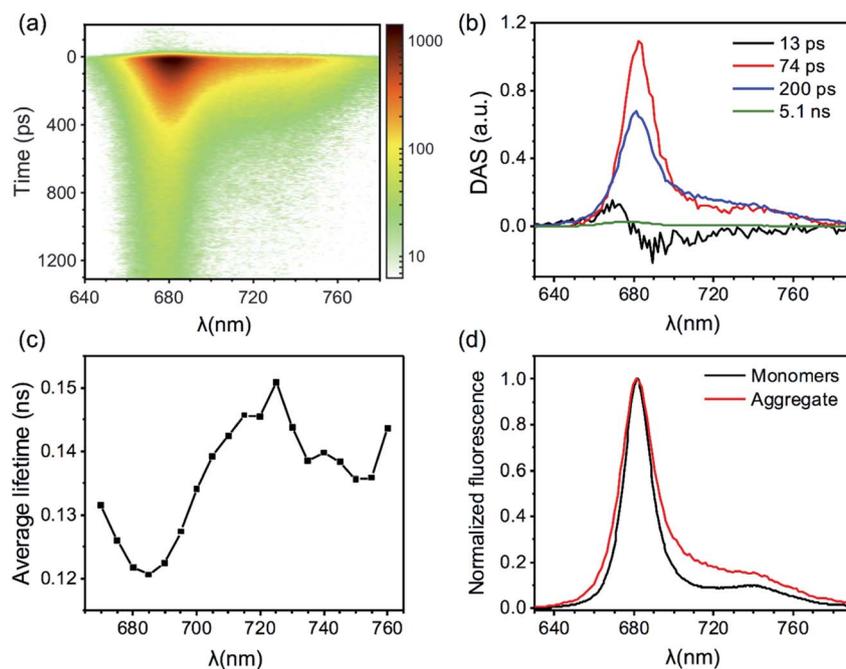

Fig. 2 TRF of CP29 oligomers at RT. (a) 2D representation (in logarithmic scale) of measured TRF data of CP29 WT excited at 400 nm and detected in the Chl Qy region. (b) DAS from global analysis of the data in (a). (c) Average Chl excited state lifetime in CP29 oligomers (calculated as $\tau_{\mathrm{avg}} = \sum_k P_k \tau_k / \sum_k P_k$, where P_k is the amplitude of the component associated with the lifetime τ_k) at different wavelengths. Only the 74 ps and the 200 ps components, representing excited state relaxation in the aggregate, were used for calculating the average lifetime (see text for details). The standard deviation on the average lifetime is ±3 ps. (d) Overlay of the time–integrated fluorescence of CP29 oligomers and of the steady-state fluorescence spectrum of CP29 monomers.
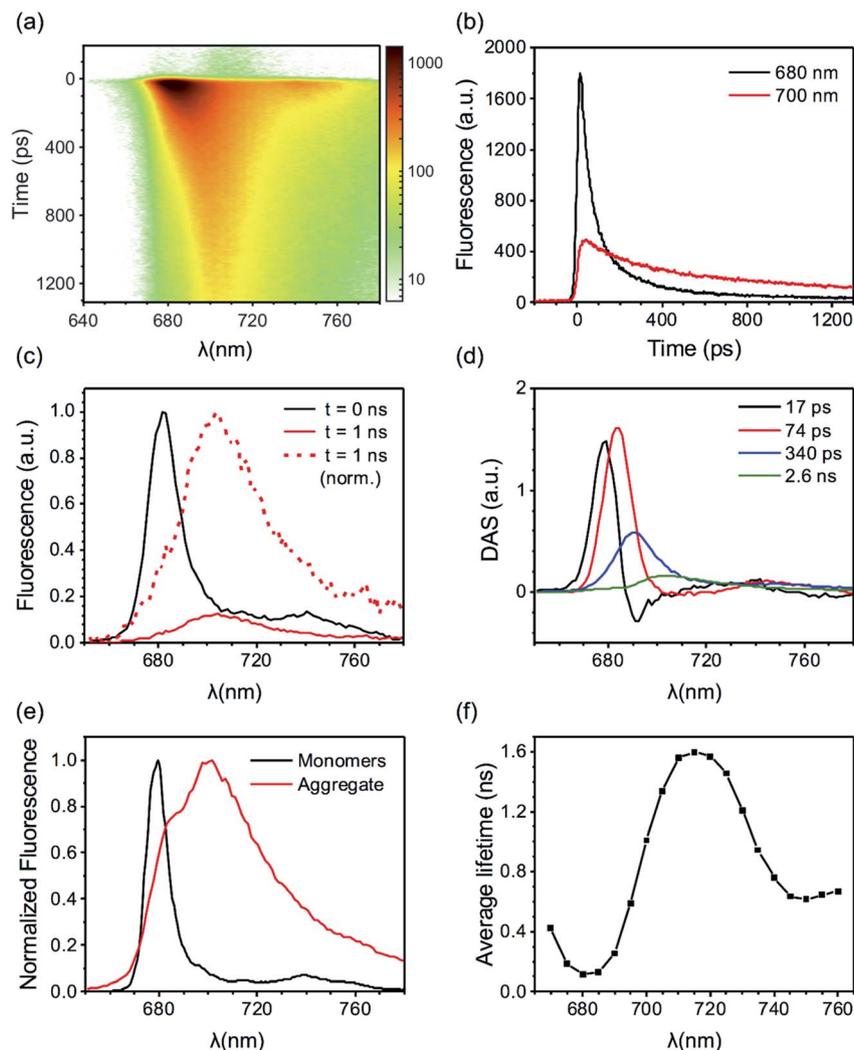
Fig. 3 TRF of CP29 oligomers at 77 K. (a) 2D representation (in logarithmic scale) of measured TRF data of CP29 WT excited at 400 nm and detected in the Chl Qy region. (b) Time traces of data in (a) at 680 nm (black) and 700 nm (red). (c) Fluorescence spectra immediately after excitation (black) and at 1 ns delay (solid red, and normalized in dashed red). (d) DAS from global analysis of the data in (a). (e) Average Chl excited state lifetime of oligomeric CP29 (calculated as $\tau_{avg} = \sum_k P_k \tau_k / \sum_k P_k$, where P_k is the amplitude of the component associated with the lifetime τ_k) at different wavelengths. The average lifetime was calculated excluding the fastest component (which has a significant energy–transfer character), but including the second one (which is mostly positive and therefore represents mainly decay processes). (f) Overlay of the time–integrated fluorescence of CP29 oligomers and of the steady state fluorescence spectrum of CP29 monomers.

that are qualitatively similar to those previously obtained for the oligomers of LHCII.[6,23,33] Such kinetics were interpreted in term of a heterogeneous picture where the LHC units in the aggregate can be found in different emissive states, characterized by different spectra and/or lifetimes, similar to what previously observed in single-molecule[4,17,18] and bulk[5,6,20–22] experiments on isolated LHCs. The spectral evolution in the aggregate reflects therefore excitation energy dissipation and transfer between different LHC units following light absorption. Most units in the aggregate must emit at 680 nm, as the time-zero spectrum is reminiscent of the spectrum of monomeric CP29 (both at RT and 77 K, see the first Evolution Associated Spectrum, EAS, in Fig. S4c and d†). However, due to protein clustering, the initial excitation can hop from the majority of the 680 nm centers to

a minority of centers with different emissive properties, such as dissipative (short-lived) centers and/or redshifted centers. At 77 K, when uphill energy transfer is thermodynamically unlikely, fluorescence gradually decays and redshifts across different timescales and spectral components (see Fig. 3a and d and EAS in Fig. S4d and f†). The energy equilibration from the whole aggregate to the red-emitting centers is, however, only partial, as the maximum amplitude of the time-trace at 700 nm is more than three times smaller than that at 680 nm (Fig. 3b). Due to their nearly irreversible trapping, the red-emitting states show a rather long lifetime, in the nanosecond range (see the green DAS in Fig. 3d). Consequently, other short-lived centers must compete with the red-emitting ones for excitation trapping in the aggregate. This trend is less evident at RT where, even

though the decay is still slightly slower in the far-red region than in the blue (Fig. 2c), the overall kinetics is dominated by the 680 nm emitters at all times (Fig. 2a, b and S4c, e†) and fluorescence almost entirely decays in few hundreds of picoseconds at all wavelengths. These findings can be explained by uphill energy transfer becoming more favorable at higher temperatures and making the trapping by red states more reversible. Energy dissipation by the additional quenching centers becomes therefore more efficient. The measurements performed on CP29 monomers are compatible with the described model, as the red-emitting isolated complexes appear to be long-lived at 77 K (see average lifetimes around 700 nm in Fig. S3d†). These experiments also provide a valid candidate for the strong quenching centers, *i.e.* the 680 nm short-lived complexes observed at both RT[22] and 77 K (Fig. S3a and b†).

Extracting the signatures of different fluorescent states from the data

In order to apply the above-described heterogeneous picture, the fluorescence data were further analyzed by means of multivariate curve resolution (MCR, see Methods section and Chmeliov et al.[6] for details). This approach helps disentangling the contributions of the different emissive states involved in the measured kinetics, obtaining their relative spectra (Species Associated Spectra, SAS(λ)) and population kinetics $C(t)$. Three components were required to successfully reproduce the experimental data from aggregated CP29 at 77 K (see Fig. S5 and S6† for details). The spectra of these three components, reflecting three distinct fluorescent states of CP29 units in the aggregate, have peaks at about 680, 690 and 700 nm, respectively (Fig. 4a). These states will be referred to as blue, intermediate and far-red (FR) hereafter. The corresponding kinetic traces are shown in Fig. 4b and represent the time-dependent population of each species after excitation. The traces were scaled so that all SAS had the same area, which implies that the oscillator strength of all these states is the same (supported by the evidence that the emitting dipole strength in LHCa's is similar to that of LHCb's).[12,13] The population of the blue complexes has the largest initial amplitude, rises on the time scale of the instrument response function (IRF) and shows the fastest decay (Fig. 4b, blue trace). This indicates that blue complexes represent the majority of units in the aggregate and quickly decay due to energy transfer and/or dissipation. Conversely, the two redshifted species (green and red traces) display a slower rise, meaning that they receive excitations from blue complexes, and also have a longer lifetime, a trend which is particularly emphasized in the FR species. The maximum of the red trace in Fig. 4b is 150 ps delayed with respect to that of the blue trace, showing that excitations can diffuse in the aggregate over quite long timescales. The maxima reached by the traces of the intermediate and FR species are, however, below half of that of the blue species, confirming that the amount of excitations reaching the red-emitting centers represents only part of the total initial excitation and that a number of short-lived centers must be present. The longer lifetime of the two redshifted species indicates that the quenching units have a spectrum

more similar to that of the shorter-lived blue species. Interestingly, the spectrum of the blue component overlaps fairly well with the steady-state spectrum of monomeric CP29 (Fig. 4c). In addition, both quenched and unquenched monomeric antennae display a fluorescence spectrum essentially identical to each other[22] (and to the steady-state spectrum, see also Fig. S3a and b†). This supports the hypothesis that the blue species observed in the aggregate stem from the same strongly quenched and unquenched states found in the isolated form of CP29. In this view, the contributions from the blue unquenched and quenched complexes would add up to produce the blue trace in Fig. 4b.

Three components can be also extracted from the RT data of CP29 oligomers (see Fig. S7 and S8† for details). One of these components, with a spectrum blue-shifted to 674 nm and a kinetic trace with very small amplitude and long lifetime (magenta SAS/trace in Fig. 4d and e) can be assigned to a minor fraction of unconnected pigments/antennae (<5% of the total initial amplitude) and is therefore neglected in the following analysis. The smaller difference between the decay traces at 680 and 700 nm is such that the overall kinetics is dominated by one "blue" component at all times (blue SAS/trace in Fig. 4d and e), whereas the amplitude of the additional redshifted species is significantly reduced (red SAS/trace). The kinetic trace of the blue complexes at RT, as for that at 77 K, has a steep rise and the fastest decay (Fig. 4e). The spectrum of the redshifted component (Fig. 4d, red SAS), instead, is reminiscent of that of the FR species observed at 77 K (Fig. 4a, red SAS) and its additional broadening might be ascribed to temperature effects and, possibly, to a minor contribution from intermediate species (Fig. 4a, green SAS). The kinetic profile of this species at RT also shows a slower rise and decay compared to the blue one (compare cyan and gray lines in Fig. 4e), as for its low-temperature analogue, meaning again that red-emitting centers are populated from the 680 nm ones and that they have a longer lifetime. Furthermore, only a small fraction of initial blue excitations equilibrates with the red-emitting complexes, which indicates that most energy dissipation occurs *via* different traps. All these analogies suggest that the strongly redshifted species observed at both temperatures represent the same (FR) emissive state. In comparison to the low temperature case, however, the overall kinetics of FR centers at RT is faster and more similar to that of blue complexes (compare the red/blue traces in Fig. 4b and e). If we assume that the FR complexes maintain a long intrinsic lifetime at all temperatures (as for the constitutively red-emitting LHCa's[36]), the sizable shortening of their kinetics at RT might be explained by the higher available thermal energy making them more shallow traps. As a result, the excitations that reached the FR centers can hop back to the blue centers and be dissipated by different traps. The spectrum of the blue component matches that of CP29 monomers at RT (Fig. 4f), similarly to what is observed for the corresponding species at 77 K (Fig. 4c). This allows us to assign the blue species observed in the aggregate to the quenched/unquenched states observed in the isolated complex at both temperatures.
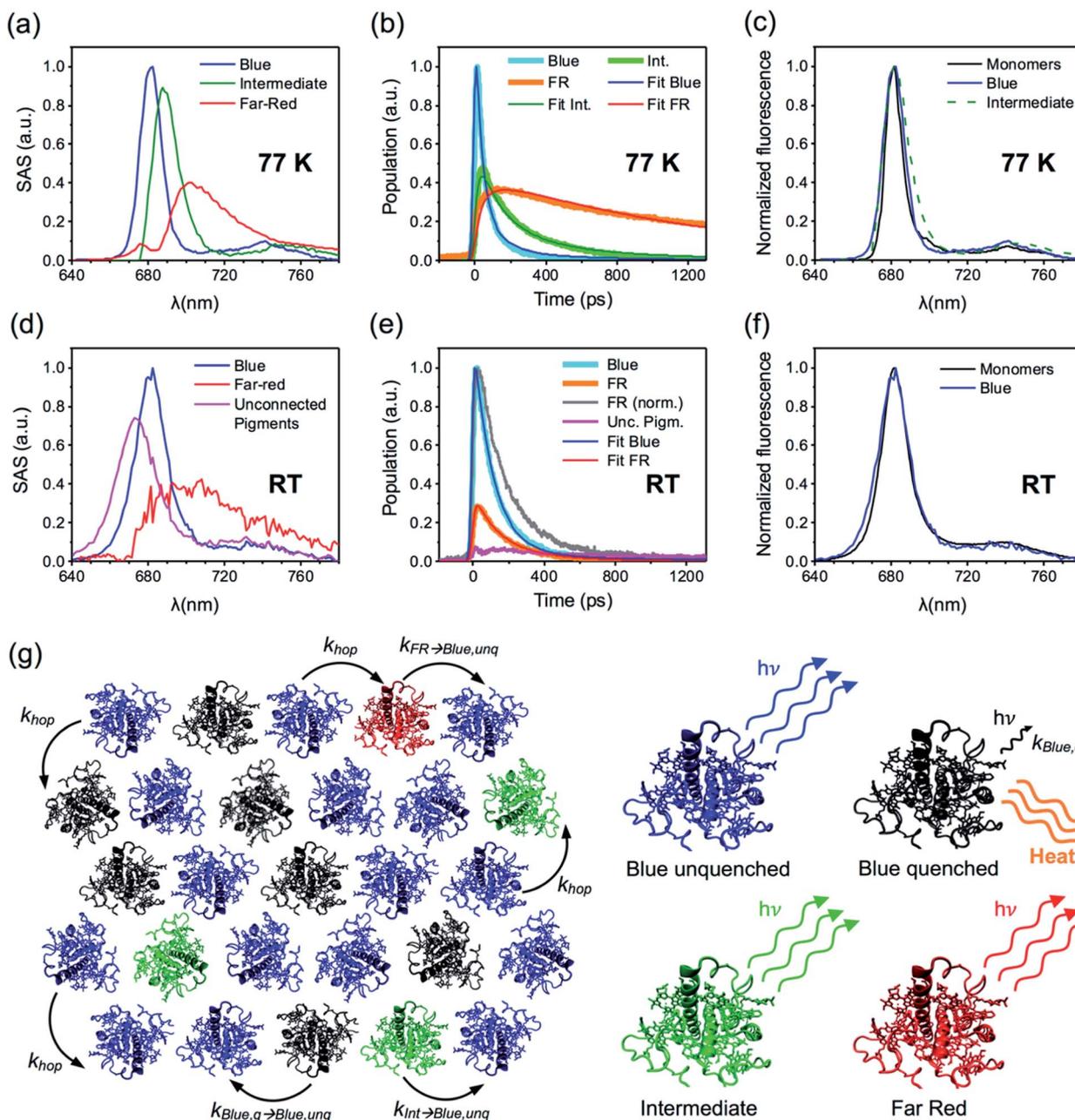
Fig. 4 Analysis and modeling of TRF data. (a) SAS of the three components from MCR of fluorescence data of CP29 oligomers at 77 K. SAS are normalized to their area. (b) Kinetic traces associated with the spectral components in (a). The traces obtained from MCR are presented in thick lines, whereas those fitted using the parameters in Table 1 are presented in thin lines. (c) Overlay of the normalized blue and intermediate SAS of panel (a) and of the steady-state spectrum of CP29 monomers at 77 K (red-shifted by 2 nm for better comparison). The spectrum of the intermediate component was blue-shifted by 6.5 nm. (d) SAS of the three components from MCR of fluorescence data of CP29 oligomers at RT. SAS are normalized to their area. (e) Kinetic traces associated with the spectral components in (d). The traces obtained from MCR are presented in thick lines, whereas those fitted using the parameters in Table 1 are presented in thin solid lines. A normalized trace for the far-red component is also displayed for better comparison with the blue trace. (f) Overlay of the normalized blue SAS of panel (d) and of the steady-state spectrum of CP29 monomers at RT. (g) Proposed hexagonal arrangement of CP29 monomers in the aggregate. Based on the specific conformation, each unit can be found in one of four different fluorescent states (see text for details): blue unquenched (the most abundant, in blue), blue quenched (in black), intermediate (in green) and far-red emitting (in red). Blue unquenched and quenched complexes are assumed to have the same emission spectrum. At room temperature, only the blue unquenched, blue quenched and far-red emitting states could be resolved by MCR. All states but the blue quenched one are assumed to be long-lived and highly fluorescent (with the lifetime fixed to 4 ns), whereas the decay rate of blue quenched complexes ($k_{\text{blue,q}}$) is a free fitting parameter in the model (see Text S1†). Inter-monomer excitation hopping rates are indicated with arrows.

Kinetic modeling sheds light on the physical nature of the fluorescent states

The previous analysis allowed us to determine the spectra of the different fluorescent states of the CP29 units in the aggregate, as well as their excited state kinetics after light absorption. However, some relevant information, such as the lifetimes of these fluorescent states and their relative abundance within the aggregate, are still missing. To extract these details from the data, we simulated the kinetic traces obtained by MCR using a coarse-grained model similar to the one previously developed for LHCII oligomers[6,33] (see Text S1† for details). As in that work, we assumed that the CP29 aggregates are organized into a 2D hexagonal lattice (Fig. 4g). The model has a CP29 complex as its smallest unit, whereas intra-monomer energy equilibration is neglected being about an order of magnitude faster than the experimental time resolution.[47–49] At RT, each CP29 complex in the aggregate can be found in one of three possible states: blue unquenched, blue quenched, or FR. At 77 K, four emissive states are possible: blue unquenched, blue quenched, intermediate, and FR (Fig. 4g). Excitations can hop between adjacent complexes with different rates based on their emissive properties. Each conformational state is characterized by a lifetime and an average occurrence in the aggregate. Together with the blue unquenched state, redshifted states were assumed to have (fixed) lifetimes of 4 ns based on the 77 K monomer and aggregate data and on the fact that the red-emitting states of the LHCa's are mainly long-lived also at RT[36] (see Text S1† for details). The fitting parameters were (i) the hopping rates between the different types of complexes, (ii) the lifetime of the blue quenched state, and (iii) the relative abundance of each state in the ensemble. The calculated kinetics were fitted to reproduce the fluorescence kinetics obtained by MCR (in the case of the blue component, the contributions from quenched/unquenched complexes were added up to fit the blue trace from MCR), yielding good fitting quality at both temperatures (see Fig. 4b and e). The obtained fitting parameters are listed in Table 1.

At RT, the blue short-lived complexes have an effective lifetime of about 80 ps, which is compatible with the lifetime of the strongly quenched state found in monomeric CP29.[22] The relative amount of (strongly) quenched complexes in the aggregate is 21% of the total, which is slightly higher than the 16% found for the monomeric state,[22] while the FR complexes represent about 14% of all units. This suggests that protein clustering increases the occurrence of quenched and FR complexes (the latter are hardly detected in the monomers, whose excited state lifetime is nearly wavelength-independent, see Fig. S3d†). The hopping times between complexes can be compared to determine their relative effective excited state free energy as $\Delta G_{AB} = G_B - G_A = k_B T \ln(\tau_{A \to B}/\tau_{B \to A})$, where k_B is the Boltzmann constant. The calculated hopping times suggest that the order of the effective excited state free energies is $G_{\text{blue,q}} < G_{\text{FR}} < G_{\text{blue,unq}}$. The blue quenched complexes are therefore very efficient energy traps, as the back transfer to unquenched complexes is unfavorable, whereas the long-lived red-emitting complexes only act as shallow traps due to their longer lifetime and the available thermal energy. At 77 K, the lifetime of the dissipative state drops to 48 ps, which is somewhat shorter than the lifetime of the quenched state in the monomers (Fig. S3a and b†). The occurrence of the quenched complexes in the aggregate (28%) is also higher than that observed in the monomeric state (18%), implying that clustering stabilizes the quenched conformation also at cryogenic temperatures. The amount of redshifted antennae is nearly 12% for the intermediate state and almost 4% for the FR state. The free energy order at 77 K is $G_{\text{FR}} < G_{\text{int.}} < G_{\text{blue,q}} < G_{\text{blue,unq}}$. As expected, the red-emitting states (and especially the FR ones) are deeper traps at 77 K than at RT, which virtually prevents excitation from returning back to the blue unquenched complexes.

The role of specific chlorophylls in light-harvesting regulation

The investigation performed so far demonstrates that energy dissipation in CP29 oligomers is due to quenching centers whose emissive properties (lifetime and spectra) are compatible with those exhibited by quenched monomeric CP29. In order to evaluate the contribution of specific chlorophylls to the quenching and to the occurrence of red-emitting states, the above-described fluorescence experiments were repeated on two

Table 1 Energy transfer lifetimes, relative occurrence and trapping lifetimes for the different emissive states observed in monomeric and aggregated CP29 at RT and 77 K. The lifetimes of the blue unquenched, intermediate and far-red species were fixed to 4 ns. For the monomer parameters, only the amplitude and lifetime of the strongly quenched blue component is shown (see TRF data in Fig. S3 and Mascoli et al.,[22] the error represents 95% confidence intervals). The lifetime and amplitude in parenthesis for the quenched monomers at RT are estimated from previous transient absorption measurements.[22] The aggregate parameters refer to the TRF data and to the model described in the text, as well as the spectral components displayed in Fig. 4a and d (the uncertainty is expressed as standard deviation). See Methods section and Text S1 for details. An additional fitting parameter was the number of long-lived unconnected complexes, which was extracted from the kinetic trace of the blue component and estimated as <1% at both temperatures. Note that, for all energy transfer acceptor–donor couples, only the lifetime for the slower (uphill) process is listed, as the lifetime of all downhill and isoenergetic transfers was fixed to 25 ps at RT and 32 ps at 77 K (see Methods section, Text S1 and Fig. S9)

	$\tau_{\text{blue,q} \to \text{blue,unq}}$ (ns)	$\tau_{\text{int.} \to \text{blue,unq}}$ (ns)	$\tau_{\text{FR} \to \text{blue,unq}}$ (ns)	% Blue,q	% Int.	% FR	$\tau_{\text{blue,q}}$ (ps)
Mon. RT	—	—	—	16 ± 1 (16)	—	—	90 ± 30 (54)
Aggr. RT	1.9 ± 0.2	—	0.44 ± 0.08	21 ± 2	—	13.9 ± 0.5	79 ± 3
Mon. 77 K	—	—	—	18 ± 2	—	—	130 ± 30
Aggr. 77 K	0.58 ± 0.09	1.7 ± 0.3	31 ± 7	28 ± 3	11.8 ± 0.3	3.8 ± 0.1	48 ± 3

chlorophyll knock-out (KO) mutants of CP29. These KO complexes lose either Chl *a*612 (and *a*611) or *a*603,[42] respectively, and are therefore referred as KO612 and KO603 hereafter. It should be noted that these two Chls, forming strongly coupled Chl *a* dimers with the neighboring Chls (*a*611 and *a*609, respectively, see Fig. 1),[41] are involved in the low energy states of the complex.[42,49] As a result, these two Chls can be expected to play a role in the quenching mechanism and/or in the occurrence of red forms. In addition, we have recently demonstrated that, at RT, only the loss of Chl *a*612 has a significant effect on quenching in the monomers, as the occurrence of short-lived complexes decreases and their decay rate is slowed down[22] (see Fig. S10 and S11† for the lifetime measurements on the monomeric KO complexes at 77 K).

The measured excited state kinetics of CP29 612/603 KO mutants are qualitatively similar to those of the WT complex. At RT, a drastic quenching is observed in the oligomers in comparison to the monomeric form (see DAS in Fig. S12 and S13†). Energy dissipation is still slightly faster at 680 nm than at 700 nm (see Fig. S12 and S13† for the wavelength-dependent average lifetimes). Similarly, at 77 K, energy dissipation and equilibration towards the red proceed in parallel through different timescales and spectral forms (Fig. S14 and S15†). Some quantitative differences with the WT aggregates, however, can be noticed from the data. The overall trapping appears to be slowed down in the KO612 oligomers (compare, for instance, Fig. 2b, c and S12a, b†), which is in agreement with the level of quenching being reduced in the KO612 monomers at RT[22] and 77 K (Fig. S11†). On the other hand, quenching in the KO603 aggregates is even faster than in the WT aggregates, especially at RT (*cf.* Fig. 2b, c and S13a, b†). This experimental evidence is more difficult to interpret, as the level of quenching in the KO603 monomers at RT was shown to be similar to that of the WT.[22] Furthermore, an enhancement of the far-red emission is still observed in the steady-state and time-resolved data of the aggregates in comparison to the KO isolated complexes. However, the amount of red forms appears to be significantly reduced in both KO612 and KO603 aggregates with respect to the WT ones, especially at 77 K (see Fig. 5 and S16† for the RT data).

MCR was applied to the mutant data as well, yielding again two aggregate-related components at RT (the same blue and FR states found in the WT), and three (the same blue, intermediate and FR states found in the WT) at 77 K (see Fig. S17–S26 in the ESI† for details). The spectra and concentration profiles of these species are comparable to those obtained for CP29 WT oligomers. The experimental traces were also fitted to determine other relevant parameters for the different fluorescent states highlighted by MCR. These parameters are listed in Tables S1 and S2.† In both mutants, it is still possible to assign the role of quenchers to the blue centers, whose spectrum is equivalent to that of unquenched blue centers and to the spectrum of the monomeric complexes (see Fig. S20, S21, S25 and S26†). Moreover, the fitted excited state free energies show the same trends found for CP29 WT at both RT and 77 K (see Tables S1 and S2†). However, if in CP29 WT aggregates the number and lifetime of the quenched complexes are fairly close to those
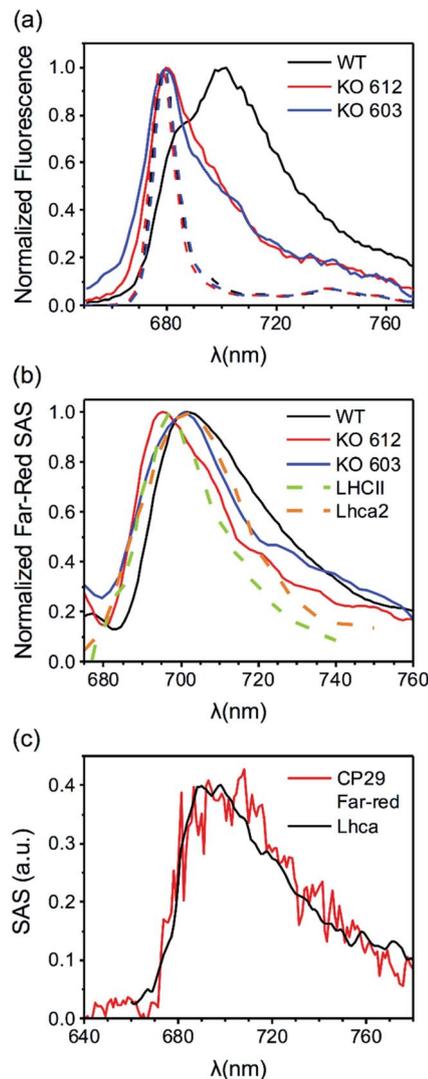

Fig. 5 (a) Far-red contributions from fluorescence spectra of CP29 WT and KO mutants (see Fig. 3, S14 and S15† for the time-resolved data). Solid lines: time-integrated fluorescence spectra of CP29 (WT and KO mutants) oligomers at 77 K. Dashed lines: steady-state fluorescence spectra (500 nm excitation) of CP29 (WT and KO mutants) monomers at 77 K. (b) Far-red SAS (normalized to their maxima) extracted from 77 K data of CP29 WT, KO612 and KO603 (see Fig. 4a, S20 and S21† for the full sets of SAS). Far-red SAS of LHCII oligomers at 80 K (from Chmeliov et al.[6]). 77 K emission spectrum of Lhca2 (from Croce et al.[50]). (c) Far-red SAS extracted from RT data of CP29 WT (red line, see Fig. 4d) and Lhca-like spectrum from target analysis of RT fluorescence data of PSI–LHCI of the green alga *Chlamydomonas reinhardtii* (from Le Quiniou et al.[51]).

observed in the monomeric state, this trend is not clearly reproduced in the KO612/603 oligomers. The amount of traps, for instance, increases more drastically in CP29 KO603 upon aggregation, thus explaining the faster quenching observed for this sample (Table S2†). In addition, the lifetime of the quenched KO612 complexes in the aggregate becomes significantly shorter than that of isolated KO612 complexes, at least at 77 K (Table S1†). For both mutants, however, the fitting consistently predicts a reduced amount of FR complexes in

comparison to CP29 WT aggregates at both temperatures (compare Table 1 to Tables S1 and S2†), which confirms that both KO612 and KO603 CP29 partially lose their capability to switch to the red-emitting states. At the same time, the amount of red forms does not correlate with the extent of quenching, which in the KO603 aggregates is even stronger than in the WT ones. This represents further evidence of the fact that red-emitting states are not involved in quenching.

Discussion

Variety of emitting conformational states

Our results indicate that CP29 aggregates represent a very heterogeneous system where the interplay between different emissive states translates into a variety of spectral components and timescales for the excited state kinetics. An analogous heterogeneity (in terms of both fluorescence spectra and lifetimes) has been previously reported for isolated LHCs by means of single-molecule[4,17,18] and ensemble[20,22,36] experiments. Here, the information extracted by MCR and simulations provide us with valuable insights into the physical origin of the different fluorescent states observed in the aggregate. This knowledge can be combined with that of monomeric CP29 from our previous work[22] to answer physiologically relevant questions on how the conformational landscape of LHCs is modulated under different environmental conditions. The previously-discussed blue species detected in the aggregate data include contributions from two different states – one quenched and one long-lived – with a fluorescence spectrum that is very similar to that of CP29 monomers. Furthermore, the short-lived (quenching) complexes display nearly irreversible trapping, a property that was also observed in LHCII oligomers.[6] The spectrum of the quenched state has the typical features of a chlorophyll excitonic state and implies that the quencher is a dark state accepting energy directly from chlorophylls. The strong trapping character also suggests that energy transfer from chlorophylls to the quencher within the short-lived complexes is rather fast and unidirectional. Quenching in monomeric CP29 exhibits the exact same features and is caused by fast excitation energy transfer from chlorophylls to a carotenoid dark state.[22] The lifetime and spectrum of the short-lived complexes present in the aggregate (as estimated from the fitting) are also compatible with those (experimentally determined) of quenched CP29 monomers.[22] All these pieces of evidence represent a solid proof that CP29 exhibits equivalent emissive states in two very different environments, i.e. when detergent-solubilized as a monomer and upon clustering. This indicates that the quenching mechanism promoting efficient energy dissipation in the aggregates is the same active in the isolated complexes, that is, chlorophyll-to-carotenoid excitation energy transfer. This evidence also suggests that a similar conformational landscape might be adopted in the membrane and that an analogue quenching mechanism might play a role in the photoprotective response of plants against excess light. Notably, while oligomerization results in a relative increase of quenched complexes (Table 1), the large majority of CP29 units remains in a long-lived state (blue- of FR-emitting). This proves

that the strong quenching achieved in the aggregates does not require a drastic increase in the number of quenchers. Even though aggregation can possibly stabilize the quenched conformation (as further supported by the CP29 KO mutant data), the energetic connectivity resulting from protein clustering is such that a relatively small amount of strong traps is sufficient to effectively quench excitations in the whole aggregate.

Besides quenching, the other spectroscopic signature standing out from the aggregate data is the enhanced emission in the far-red region. This contribution stems from a minor fraction of red-emitting and relatively long-lived complexes. Despite their lower amount, these redshifted antennae can accept excitations from the blue ones and, due to their lower excited state energy, they represent alternative traps to the short-lived blue complexes, implying that they can be still populated to a significant extent. Unsurprisingly, the trapping efficiency of redshifted states is strongly temperature-dependent. At 77 K they act as strong energy sinks and significantly slow down the excited state kinetics in the far-red region (compare Fig. 2 and 3). As a result, the steady-state fluorescence exhibits a sizeable enhancement in the far-red spectral region (Fig. 5a). At RT, where uphill energy transfer becomes more favorable, redshifted complexes become shallow traps and are outcompeted by blue quenched complexes. Their contribution to the overall kinetics becomes less visible, as their lifetime is significantly reduced by de-trapping and quenching by blue centers. A similar trend was also observed for LHCII oligomers, where the red-emitting component could only be resolved at temperatures up to 200 K.[6] However, at variance with that work, where at cryogenic temperatures only one redshifted form was observed, in CP29 oligomers we were able to resolve two different red-emitting states (referred as intermediate and far-red in the results section), indicating that the energy landscape of this LHC is very diverse.

Molecular origin of the red-emitting and quenching states

The spectrum of the red-most species peaks around 700 nm and is very broad, resembling that resolved for LHCII oligomers at low temperatures[6] (see Fig. 5b). It is also reminiscent of the emission spectra of the LHCa's[36,50,51] (Fig. 5b and c), whose spectral redshift and broadening are interpreted in terms of a Chl–Chl charge transfer (CT) state mixing with the manifold of Chl excitonic states.[52] Our measurements also reveal that the red-emitting states found in CP29 are relatively long-lived, in agreement with what reported for LHCa's.[36] The FR component resolved in our measurements at both RT and 77 K can be therefore explained with the presence of a low-energy Chl–Chl CT state within the excited state manifold of this distinct CP29 fluorescent state. This assignment is also in agreement with Stark fluorescence measurements performed on oligomeric LHCs.[35,53] The physical origin of the intermediate state is somewhat more difficult to establish. Its spectral broadening is less pronounced and, when blue-shifted, its spectrum still overlaps to a good extent with that of the blue state (Fig. 4c). In addition, the spectral redshift of the intermediate species is

limited to less than 7 nm with respect to its blue counterpart (and is even reduced in the KO mutants, see Fig. S20 and S21†). This modest redshift (which is still enough for the intermediate state to act as a deep trap at 77 K) might result from a purely excitonic state whose energy is lowered by some specific realizations of protein disorder.[54] However, we cannot completely rule out the hypothesis that a smaller degree of CT character is responsible for the redshift, as the spectra of some LHCa's also have similar peak positions.[11,51]

Another long-standing question regarding the spectroscopy of LHCs is the role of selected Chls in the mechanisms of quenching and fluorescence redshift. In a previous work, we showed that quenching in monomeric CP29 is sensitive to the removal of Chl $a612$, indicating that this Chl and the adjacent Lutein in the L1 binding site are key players in the energy dissipation.[22] However, these data also suggested that more than one quenching site must be present in the complex, as removal of Chl $a612$ slows down the quenching but does not suppress it. The aggregate data confirm these findings. Quenching is indeed slowed down in the KO612 aggregates but remains very effective, indicating that the Chl $a612$ – Lutein 1 couple is the most efficient quenching site, but not the only potential one. The mutant data also shed light on the role of specific chlorophylls in the regulation of the photoprotective response. Indeed, the WT complex maintains a fairly similar decay rate of the quenched complexes in both the monomeric and the oligomeric state, especially at physiological temperatures, while the number of quenchers does not change drastically. This tendency is somehow altered in the mutants, were the amount and/or rate of the quenched complexes increase more substantially upon aggregation, implying that clustering stabilizes their quenched state to a larger extent. These results suggest that a full pigment complement is necessary for CP29 to preserve a robust conformational landscape, whereas the loss of selected Chls makes this LHC more sensitive to the environment. In this respect, LHCII, which is barely quenched in its trimeric form but develops a significant amount of quenchers upon oligomerization, resembles the CP29 KO mutants more than WT complexes. This difference in flexibility might be a consequence of the different pigment content of LHCII, whose low energy states are concentrated on Chls $a610$–$a611$–$a612$ only (as in CP29 KO603), whereas in WT CP29 there are more low-energy Chls.[49]

The mutants also display a lower extent of red-shifted emission upon clustering. Notably, this feature seems not to correlate with the amount of quenching, as the KO603 oligomers are the most quenched and, at the same time, emit significantly less long-wavelength photons than the WT ones. Despite the aforementioned differences, the enhancement of redshifted emission upon clustering is shared by CP29 WT and KO mutants. The removal of either Chl $a612$ or $a603$, therefore, does not fully abolish the capability of CP29 to switch to red-emitting states, even though the amount of red emission is reduced in both cases (see Fig. 5a and Tables 1, S1 and S2†). These results provide new insights on the potential location of red-forms in LHCs. Indeed, the most reasonable candidates for the redshifted Chls in CP29 are the strongly coupled Chl a dimers revealed by structural data,[41,55] that is, Chl $a611$–$a612$ and/or Chl $a603$–$a609$, as the stabilization of a CT state requires a strong interaction between the involved Chls. Furthermore, the red forms of the LHCa's have been specifically ascribed to the Chl $a603$–$a609$ dimer,[56] which suggests that the same dimer could be responsible for the redshifted emission also in CP29. Our findings deviate somehow from these predictions and suggest that both Chl $a611$–$a612$ and Chl $a603$–$a609$ pairs are capable of forming a red-emitting CT state. Indeed, the amount of red-emitting complexes is nearly halved by either Chl $a612$ or Chl $a603$ removal. Moreover, the spectrum of the red-shifted species is sensitive to the mutations, especially in the KO612 aggregates, where it significantly blue-shifts (Fig. 5b), indicating that the red-most forms might be associated to the Chl $a611$–$a612$ dimer. To sum up, the comparison of WT and mutant data indicates that multiple potential quenching and red-emitting sites are present within the same LHC. In addition, the amount of red-shifted emission observed upon aggregation does not correlate with the extent of quenching, which represents an additional proof that far-red emitting states are not responsible for the strong quenching.

Conclusions

Our data show that aggregates of CP29 display a high degree of spectral heterogeneity, resulting from the different fluorescence properties of their units. This variability is already present in the monomeric form of the complex but is easier to capture in its oligomeric state, as the energetic connectivity caused by protein clustering can enhance spectroscopic signatures of quenched and red-shifted states, despite their reduced occurrence. The performed bulk experiments and successive analysis allowed the identification of the different emissive states of CP29 complexes in the aggregates, which could be mapped onto the quenched and unquenched states also observed in the detergent-solubilized monomers. In view of these results, the massive quenching observed upon LHC clustering can be largely ascribed to the same long-lived and quenched complexes becoming energetically connected. The predominant quenching mechanism active in CP29 aggregates is therefore concluded to be the same previously observed in the monomers, $i.e.$, fast chlorophyll to carotenoid energy transfer. Aggregation can stabilize the quenched conformation by increasing its occurrence or reducing its lifetime, but a relatively small amount of strong quenchers is already sufficient to achieve a high extent of energy dissipation. Besides quenching, oligomerization also involves an enhanced contribution from red-emitting complexes in the fluorescence kinetics. These states are here shown not to be involved in quenching as their lifetime is significantly longer than the timescale of energy dissipation. The high resemblance of the redshifted state detected in CP29 oligomers with those exhibited by LHCa's is a witness of the common architecture shared by all members of the LHC superfamily. Despite their different structures, pigment content and location in the photosynthetic machinery, they all share the capability to switch between blue- and red-emitting states. The high tunability of pigment–protein interactions, however, is

essential in defining the extent to which each of these states is stabilized, as witnessed by the different emissive properties exhibited by LHCa's and LHCb's in bulk measurements. Despite the predominant "blue" character of the LHCb's, however, a smaller amount of red-emitting complexes in the ensemble seems to be unavoidable, at least under certain conditions. Furthermore, results from chlorophyll-deficient mutants of CP29 demonstrate that multiple potential quenching and red-emitting sites can coexist in the same LHC, which is another proof of the robustness of their architecture. Finally, the evidence that the same emissive states are observed in rather different *in vitro* environments suggests that the same states (and therefore, the same quenching mechanism) are adopted by LHCs in the membrane, despite being possibly regulated in a different way.

Conflicts of interest

The authors declare no competing interests.

Acknowledgements

Notes and references

1 S. Jansson, *Trends Plant Sci.*, 1999, **4**, 236–240.

2 A. A. Pascal, Z. Liu, K. Broess, B. van Oort, H. van Amerongen, C. Wang, P. Horton, B. Robert, W. Chang and A. Ruban, *Nature*, 2005, **436**, 134–137.

3 T. P. J. Krüger, C. Ilioaia, M. P. Johnson, A. V. Ruban and R. Van Grondelle, *Biochim. Biophys. Acta, Bioenerg.*, 2014, **1837**, 1027–1038.

4 G. S. Schlau-Cohen, H. Y. Yang, T. P. J. Krüger, P. Xu, M. Gwizdala, R. Van Grondelle, R. Croce and W. E. Moerner, *J. Phys. Chem. Lett.*, 2015, **6**, 860–867.

5 L. Tian, E. Dinc and R. Croce, *J. Phys. Chem. Lett.*, 2015, **6**, 2339–2344.

6 J. Chmeliov, A. Gelzinis, E. Songaila, R. Augulis, C. D. P. Duffy, A. V. Ruban and L. Valkunas, *Nat. Plants*, 2016, **2**, 16045.

7 J. M. Briantais, *Photosynth. Res.*, 1994, **40**, 287–294.

8 X.-P. Li, P. Muller-Moule, A. M. Gilmore and K. K. Niyogi, *Proc. Natl. Acad. Sci. U. S. A.*, 2002, **99**, 15222–15227.

9 G. Bonente, B. D. Howes, S. Caffarri, G. Smulevich and R. Bassi, *J. Biol. Chem.*, 2008, **283**, 8434–8445.

10 B. Koehne, G. Elli, R. C. Jennings, C. Wilhelm and H. W. Trissl, *Biochim. Biophys. Acta, Bioenerg.*, 1999, **1412**, 94–107.

11 T. Morosinotto, S. Castelletti, J. Breton, R. Bassi and R. Croce, *J. Biol. Chem.*, 2002, **277**, 36253–36261.

12 E. Wientjes, I. H. M. Van Stokkum, H. Van Amerongen and R. Croce, *Biophys. J.*, 2011, **100**, 1372–1380.

13 E. Wientjes, G. Roest and R. Croce, *Biochim. Biophys. Acta, Bioenerg.*, 2012, **1817**, 711–717.

14 R. C. Jennings, R. Bassi, F. M. Garlaschi, P. Dainese and G. Zucchelli, *Biochemistry*, 1993, **32**, 3203–3210.

15 S. Nussberger, J. P. Dekker, W. Kühlbrandt, B. van Bolhuis, R. van Grondelle and H. van Amerongen, *Biochemistry*, 1994, **33**, 14775–14783.

16 R. Croce and H. Van Amerongen, *Photosynth. Res.*, 2013, **116**, 153–166.

17 T. P. J. Kruger, E. Wientjes, R. Croce and R. van Grondelle, *Proc. Natl. Acad. Sci. U. S. A.*, 2011, **108**, 13516–13521.

18 M. Tutkus, F. Saccon, J. Chmeliov, O. Venckus, I. Ciplys, A. V. Ruban and L. Valkunas, *Biochim. Biophys. Acta, Bioenerg.*, 2019, **1860**, 499–507.

19 M. Tutkus, J. Chmeliov, D. Rutkauskas, A. V. Ruban and L. Valkunas, *J. Phys. Chem. Lett.*, 2017, **8**, 5898–5906.

20 I. Moya, M. Silvestri, O. Vallon, G. Cinque and R. Bassi, *Biochemistry*, 2001, **40**, 12552–12561.

21 A. Natali, J. M. Gruber, L. Dietzel, M. C. A. Stuart, R. Van Grondelle and R. Croce, *J. Biol. Chem.*, 2016, **291**, 16730–16739.

22 V. Mascoli, N. Liguori, P. Xu, L. M. Roy, I. H. M. van Stokkum and R. Croce, *Chem*, 2019, **5**, 1–13.

23 J. Chmeliov, A. Gelzinis, M. Franckevičius, M. Tutkus, F. Saccon, A. V. Ruban and L. Valkunas, *J. Phys. Chem. Lett.*, 2019, 7340–7346.

24 A. V. Ruban, D. Rees, A. A. Pascal and P. Horton, *Biochim. Biophys. Acta*, 1992, **1102**, 39–44.

25 A. V Ruban, R. Berera, C. Ilioaia, I. H. M. Van Stokkum, J. T. M. Kennis, A. A. Pascal, H. Van Amerongen, B. Robert, P. Horton and R. Van Grondelle, *Nature*, 2007, **450**, 575–578.

26 Y. Miloslavina, A. Wehner, P. H. Lambrev, E. Wientjes, M. Reus, G. Garab, R. Croce and A. R. Holzwarth, *FEBS Lett.*, 2008, **582**, 3625–3631.

27 A. V. Ruban and P. Horton, *Biochim. Biophys. Acta*, 1992, **1102**, 30–38.

28 C. W. Mullineaux, A. A. Pascal, P. Horton and A. R. Holzwarth, *Biochim. Biophys. Acta, Bioenerg.*, 1993, **1141**, 23–28.

29 S. Vasil'ev, K. D. Irrgang, T. Schrötter, A. Bergmann, H. J. Eichler and G. Renger, *Biochemistry*, 1997, **36**, 7503–7512.

30 M. G. Müller, P. Lambrev, M. Reus, E. Wientjes, R. Croce and A. R. Holzwarth, *ChemPhysChem*, 2010, **11**, 1289–1296.

31 B. Van Oort, L. M. Roy, P. Xu, Y. Lu, D. Karcher, R. Bock and R. Croce, *J. Phys. Chem. Lett.*, 2018, **9**, 346–352.

32 J. Chmeliov, G. Trinkunas, H. Van Amerongen and L. Valkunas, *J. Am. Chem. Soc.*, 2014, **136**, 8963–8972.

33 A. Gelzinis, J. Chmeliov, A. V. Ruban and L. Valkunas, *Photosynth. Res.*, 2017, **135**, 275–284.

34 M. Wahadoszamen, E. Belgio, M. A. Rahman, A. M. Ara, A. V. Ruban and R. van Grondelle, *Biochim. Biophys. Acta, Bioenerg.*, 2016, **1857**, 1917–1924.

35 M. Wahadoszamen, R. Berera, A. M. Ara, E. Romero and R. van Grondelle, *Phys. Chem. Chem. Phys.*, 2012, **14**, 759–766.

36 F. Passarini, E. Wientjes, H. van Amerongen and R. Croce, *Biochim. Biophys. Acta, Bioenerg.*, 2010, **1797**, 501–508.

37 H. Staleva, J. Komenda, M. K. Shukla, V. Šlouf, R. Kaňa, T. Polívka and R. Sobotka, *Nat. Chem. Biol.*, 2015, **11**, 287–291.

38 N. Liguori, P. Xu, I. H. M. Van Stokkum, B. Van Oort, Y. Lu, D. Karcher, R. Bock and R. Croce, *Nat. Commun.*, 2017, **8**, 1994.

39 L. Tian, P. Xu, V. U. Chukhutsina, A. R. Holzwarth and R. Croce, *Proc. Natl. Acad. Sci. U. S. A.*, 2017, **114**, 4828–4832.

40 Z. Liu, H. Yan, K. Wang, T. Kuang, J. Zhang, L. Gui, X. An and W. Chang, *Nature*, 2004, **428**, 287–292.

41 X. Su, X. Wei, D. Zhu, W. Chang and Z. Liu, *Science*, 2017, **357**, 815–820.

42 P. Xu, L. M. Roy and R. Croce, *Biochim. Biophys. Acta, Bioenerg.*, 2017, **1858**, 815–822.

43 B. Van Oort, A. Amunts, J. W. Borst, A. Van Hoek, N. Nelson, H. Van Amerongen and R. Croce, *Biophys. J.*, 2008, **95**, 5851–5861.

44 I. H. M. van Stokkum, D. S. Larsen and R. Van Grondelle, *Biochim. Biophys. Acta, Bioenerg.*, 2004, **1657**, 82–104.

45 A. Gelzinis, Y. Braver, J. Chmeliov and L. Valkunas, *Lith. J. Phys.*, 2018, **58**, 295–306.

46 Y. Braver, A. Gelzinis, J. Chmeliov and L. Valkunas, *Chem. Phys.*, 2019, **525**, 110403.

47 J. M. Salverda, M. Vengris, B. P. Krueger, G. D. Scholes, A. R. Czarnoleski, V. Novoderezhkin, H. Van Amerongen and R. Van Grondelle, *Biophys. J.*, 2003, **84**, 450–465.

48 R. Croce, M. G. Müller, R. Bassi and A. R. Holzwarth, *Biophys. J.*, 2003, **84**, 2508–2516.

49 V. Mascoli, V. Novoderezhkin, N. Liguori, P. Xu and R. Croce, *Biochim. Biophys. Acta, Bioenerg.*, 2020, **1861**, 148156.

50 R. Croce, T. Morosinotto, J. A. Ihalainen, A. Chojnicka, J. Breton, J. P. Dekker, R. Van Grondelle and R. Bassi, *J. Biol. Chem.*, 2004, **279**, 48543–48549.

51 C. Le Quiniou, L. Tian, B. Drop, E. Wientjes, I. H. M. Van Stokkum, B. Van Oort and R. Croce, *Biochim. Biophys. Acta, Bioenerg.*, 2015, **1847**, 458–467.

52 E. Romero, M. Mozzo, I. H. M. Van Stokkum, J. P. Dekker, R. Van Grondelle and R. Croce, *Biophys. J.*, 2009, **96**, L35–L37.

53 A. Kell, X. Feng, C. Lin, Y. Yang, J. Li, M. Reus, A. R. Holzwarth and R. Jankowiak, *J. Phys. Chem. B*, 2014, **118**, 6086–6091.

54 T. P. J. Krüger, V. I. Novoderezhkin, C. Ilioaia and R. Van Grondelle, *Biophys. J.*, 2010, **98**, 3093–3101.

55 X. Pan, M. Li, T. Wan, L. Wang, C. Jia, Z. Hou, X. Zhao, J. Zhang and W. Chang, *Nat. Struct. Mol. Biol.*, 2011, **18**, 309–315.

56 T. Morosinotto, J. Breton, R. Bassi and R. Croce, *J. Biol. Chem.*, 2003, **278**, 49223–49229.